

Variability and Distribution of Nighttime Equatorial to Mid Latitude Ionospheric Irregularities and Vertical Plasma Drift Observed by FORMOSAT-5 Advanced Ionospheric Probe In-Situ Measurements from 2017 – 2020

Loren C. Chang^{1,2}, Yueh-Chun Hsieh^{1,2}, Chi-Kuang Chao^{1,2}, Yi Duann^{1,2}, Cornelius Csar Jude H. Salinas^{1,2,3,4}, Jann-Yenq Liu^{1,2}, Charles C.H. Lin⁵.

¹ Department of Space Science and Engineering, National Central University, 300 Zhongda Road, Zhongli District, Taoyuan City, 320, Taiwan

² Center for Astronautical Physics and Engineering, National Central University, 300 Zhongda Road, Zhongli District, Taoyuan City, 320, Taiwan

³ NASA Goddard Space Flight Center, Greenbelt, MD, 20771, USA

⁴ Goddard Earth Sciences Technology and Research II, University of Maryland, Baltimore County, Baltimore, MD, USA

⁵ Department of Earth Sciences, National Cheng Kung University, 1 University Road, Tainan City, 701, Taiwan

*Corresponding Author: Loren C. Chang (Email: loren@g.ncu.edu.tw)

Abstract

Irregularities in ionospheric plasma distribution can result in severe scintillation and disruption to the radio frequencies utilized for satellite communications and navigation. In the low and mid latitudes, these irregularities can include Equatorial Plasma Bubbles (EPBs) and Travelling Ionospheric Disturbances (TIDs). EPBs are irregularities manifesting in low latitude nighttime ionosphere plasma density that can extend along magnetic field lines with zonal scales

on the order of 100 km or less, while TIDs are propagating wave disturbances. High frequency in-situ measurements of ionospheric plasma aboard spacecraft in Low Earth Orbit (LEO) are a direct measurement of irregularities in plasma density and are therefore valuable for resolving EPB and TID occurrences, variability, and relation to other ionospheric parameters that are believed to play a driving role in the formation of such irregularities. In this study, we utilize observations taken over a three-year period between 2017 – 2020 by the Advanced Ionospheric Probe (AIP) carried aboard the FORMOSAT-5 satellite to examine the spatial, seasonal, and interannual variability of equatorial to mid latitude ionospheric irregularities and vertical ion drift during this time. AIP provides in-situ measurements of ion density and vertical ion drift in the equatorial to mid latitude ionosphere at approximately 720 km altitude with local times between 22:00 – 23:00 local time. Our global scale results resolve distinct and inter-annually recurrent seasonal patterns in the distribution of nighttime ionospheric irregularities and vertical plasma drift during this time. Elevated occurrences of ion density irregularities are resolved along the Equatorial Ionization Anomaly (EIA) latitudes, while notable occurrences with variability consistent with EPBs also observed along the low and equatorial magnetic latitudes. Zonal variability of equatorial irregularities consistent with the signatures of nonmigrating atmospheric tides are observed. It is also notable that the occurrences and geographic distribution of ion density irregularities showed a considerable level of interannual variability, especially at mid latitudes over the South Atlantic and Southern African sectors, which showed much higher levels of irregularities in 2017 - 2018, compared to 2019 and 2020. In comparison, the spatial and interannual variation of the co-located vertical ion drifts were much more consistent during the years examined, indicating that the driver for the observed interannual variability in ion density irregularities cannot be attributed to the vertical ion drift at the same time and location of the observations. This highlights the need for in-situ instruments distributed across multiple satellites in different local time zones.

Key Words: Ionosphere, irregularity, in-situ measurements, seasonal variability, inter-annual variability, Advanced Ionospheric Probe.

1. Introduction

The implementation of satellite communications and navigation requires the propagation of radio waves through the diffuse plasma of the Earth's ionosphere (roughly 60 – 1000 km altitude), which is comprised of plasma formed through the photoionization of the neutral thermosphere (roughly 90 – 1000 km altitude) and mesosphere (roughly 60 – 90 km altitude) due to the absorption of solar extreme ultraviolet radiation (EUV). Due to the change in propagation medium from the near vacuum of space through the different layers of the atmosphere and ionosphere, as well as horizontal and vertical variations in ionospheric plasma density, trans-ionospheric radio signals are subject to refraction and diffraction. The latter can cause rapid fluctuations in the amplitude and phase of the received signal that can result in the loss of lock in severe cases – a phenomena referred to as scintillation, which is caused by propagation through localized irregularities in ionospheric plasma density (International Telecommunication Union, 2019). These ionospheric effects are particularly of concern for radio frequency (RF) communications at frequencies less than 10 GHz, which includes the VHF, UHF, L, S, C, and X-bands that are commonly used for satellite communications and navigation (International Telecommunication Union, 2017) (NASA Small Spacecraft Systems Virtual Institute, 2021). With the growing pervasiveness and usage of satellite communications and navigation technology, understanding the spatial and temporal variability of ionospheric structure at planetary and local scales has become of greater interest for an ever-growing number of stakeholders.

The ionospheric irregularities that cause signal scintillation can be attributed to a few different sources and phenomena, including equatorial plasma bubbles (EPBs) and traveling ionospheric disturbances (TIDs) (Duann et al., 2020). EPBs are depletions in ionospheric plasma density that can form in the nighttime ionosphere, extending along magnetic field lines from their formation regions in the low and equatorial latitudes into higher latitudes. The vast majority of EPBs detected in past studies using in-situ satellite measurements were found to occur within 20 degrees of the magnetic equator, with horizontal scales on the order of tens to hundreds of kilometers (Burke et al., 2004). EPBs are formed as a result of a Rayleigh-Taylor instability occurring due to the dissipation of lower ionospheric layers at night and associated with strong upward vertical plasma drifts in the post sunset ionosphere (Smith et al., 2016). The molecular ions dominating the ionospheric D (roughly 60 – 90 km altitude) and E (roughly 90 – 200 km altitude) regions recombine rapidly during the local nighttime, leaving the much longer-lived atomic ions of the F region (roughly 200 – 1000 km altitude) dominating the overall plasma density in the vertical direction. The large vertical plasma gradient that results is conducive to the formation of a Rayleigh-Taylor instability triggered by perturbations, such as atmospheric gravity waves, causing the formation of EPBs as long plasma depletions extending along magnetic field lines (Sultan, 1996; Kil, 2015).

The occurrence rate of EPBs is believed to be highly correlated to mechanisms contributing to a large Rayleigh-Taylor growth rate, notably a strong vertical plasma gradient in the post sunset hours, as well as the presence of gravity wave perturbations capable of triggering the Rayleigh-Taylor instability in this unstable nighttime ionospheric configuration (Tsunoda et al., 2015). The former is closely associated with large vertical plasma drifts in the post sunset ionosphere exceeding a threshold value, which was identified as a necessary but not sufficient condition for EPB formation (Smith et al., 2016). This large vertical drift can be driven by the

pre-reversal enhancement (PRE), which was found in numerical simulations to be proportionate to solar activity and inversely proportional to nighttime E region electron densities (Fesen et al., 2000). Conditions favorable for the large post sunset vertical ion drift also show a seasonal and longitudinal dependence due to the steepest longitudinal gradient in field-line integrated Pederson conductivity occurring when the solar terminator is aligned with magnetic field lines (Tsunoda, 1985). As a result, the EPB occurrence rate has been found to be highest during the equinoxes in most longitudinal sectors where the magnetic declination is small, and during the boreal winter in the American sector, due to the larger magnetic declination angle in that region (Batista et al., 1986; Gentile et al., 2006). Deviations from this seasonal variation are present in the Central Pacific and African sectors, where the EPB occurrence rates maximize during boreal summer, which has been attributed to modulation of vertical plasma drifts by atmospheric tides in the E region with zonal wavenumber 2 in the local time frame (Tsunoda et al., 2015; Chang et al., 2021).

TIDs are propagating ionospheric wave disturbances, with medium scale TIDs (MSTIDs) having wavelengths on the order of hundreds of kilometers and large-scale TIDs (LSTIDs) having wavelengths on the order of thousands of kilometers. MSTIDs have phase speeds of roughly $400 - 1000 \text{ m s}^{-1}$, while LSTIDs have phase speeds on the order of $250 - 1000 \text{ m s}^{-1}$ (Sivakandan et al., 2021). TIDs are often associated with the signatures of atmospheric gravity waves generated in or capable of propagating into the thermosphere and ionosphere (Hocke & Schlegel, 1996), with MSTIDs being a potential trigger source for the formation of EPBs (Takahashi et al., 2018). It has been found in observations and modelling studies that LSTIDs can be generated at high latitudes as a result of energy deposition from geomagnetic storms, propagating meridionally in both directions from the auroral oval with amplitudes decreasing with equatorward propagation and maximum amplitudes occurring between the midnight and dawn sectors (Gardner & Schunk, 2010). On the other hand, the seasonal and longitudinal variation of daytime MSTIDs shows a dependency upon the variation and favorable generation conditions for gravity waves by equatorward thermospheric winds during the winter, as well as tropospheric events such as cyclones that can lead to the convective generation of gravity waves (Chen et al., 2019). Sivakandan et al. (2021) found through comparisons of Global Positioning System (GPS) derived TECs and simulations using the coupled atmosphere-ionosphere Ground-to-topside of Atmosphere and Ionosphere for Aeronomy (GAIA) model that the aforementioned equatorward wind generation mechanism produced higher levels of daytime MSTID activity during the boreal winter over the East Asian sector, and an austral winter peak over the American sector. The levels of daytime MSTID activity at different seasons and longitudes were generally correlated to variations in thermospheric meridional wind, which were attributed to gravity wave activity. On the other hand, nighttime MSTIDs tend to show different variability compared to potential gravity wave sources, suggesting other generation mechanisms. Observations have shown that nighttime MSTIDs tend to have higher occurrence rates during the solstices, but with considerably variability between the summer and winter hemispheres depending upon longitudinal sector (Makela & Otsuka, 2012; Liu et al., 2021). It has been proposed that mid latitude nighttime MSTIDs with spatial scales larger than 50 km are formed because of the Perkins instability, where perturbations in ionospheric conductivity cause the formation of polarization electric fields leading to instability generation (Makela & Otsuka, 2012).

Although the effects of ionospheric irregularities such as EPBs and TIDs can be resolved using remote sensing methods such as GNSS amplitude and phase scintillation indices from ground or satellite-based receivers, a more direct method of ionospheric irregularity observations with less complexity associated in data inversion is the use of in-situ ionospheric plasma measurements aboard satellite platforms, which sample along the spacecraft orbit (Duann et al., 2020). In-situ plasma sensors such as retarding potential analyzers and Langmuir probes have long been used to observe electric currents generated through interaction with ionospheric plasma at various electrical potentials. These “I-V curves” can be used to derive ionospheric plasma parameters such as ion and electron temperature, density, drift velocity, as well as heavy to light ion ratio and composition (Merlino, 2007). Though more limited in number and spatial coverage, especially compared to ground-based sensors, the value of such in-situ ionospheric measurements has led to the development and utilization of a variety of in-situ plasma sensor payloads that have flown aboard multiple satellite missions, which are reviewed in more detail by Duann et al. (2020).

One recent in-situ ionospheric sensor payload is the Advanced Ionospheric Probe (AIP), which was developed by National Central University in Taiwan and has been operational aboard the Taiwan Space Agency (TASA, formerly the National Space Organization or NSPO until 2023) FORMOSAT-5 satellite at a 720 km altitude Sun synchronous orbit (SSO) since 2017. AIP is an all-in-one in-situ plasma sensor combining four different operational modes in a time-sharing manner (Lin et al., 2017). The operational modes of AIP and the parameters that can be derived are as follows:

- Planar Langmuir Probe (PLP): Electron temperature.
- Retarding Potential Analyzer (RPA): Ion composition and temperature, ion ram speed, ion density.
- Ion Trap (IT): Ion density.
- Ion Drift Meter (IDM): Ion arrival angle, ion density.

The ion ram speed from RPA mode and ion arrival angle from IDM mode can further be combined with the spacecraft velocity vector to derive the relative ion drift velocity vector. AIP can operate at a sampling frequency as high as 8192 Hz, allowing for features as small as 7.4 meters to be resolved. The ion density measurement on FORMOSAT-5 is implemented in two methods: by using current measurements from RPA mode before the retarding potential is applied, or by using the total current measured in IDM mode. The independent IT mode is not actually used in current operations. The PLP is not used on orbit as it was found to have been contaminated in early operations.

Initial analysis of FORMOSAT-5 / AIP observations by Chao et al. (2020) during a few geomagnetically quiet days in December 2017 confirmed the ability of AIP to resolve large scale ionospheric features such as the midlatitude ionospheric trough in ion density, as well as longitudinal variations in ion density and vertical ion drift. In this study, we further expand on these initial results to examine the spatial, seasonal, and inter-annual variation of smaller scale ionospheric irregularities detected in AIP ion density observations, as well as the corresponding vertical ion drift from 2017 through 2020. The results are illustrative of the capabilities of AIP, as well as level of inter-annual consistency and variation in the distribution of low latitude

ionospheric irregularities such as EPBs and MSTIDs, as well as the vertical ion drift believed to be a contributing factor to the occurrence rate of EPBs.

2. Methodology

Journal Pre-proofs

The FORMOSAT-5 / AIP ion density and vertical ion drift data utilized in this study are

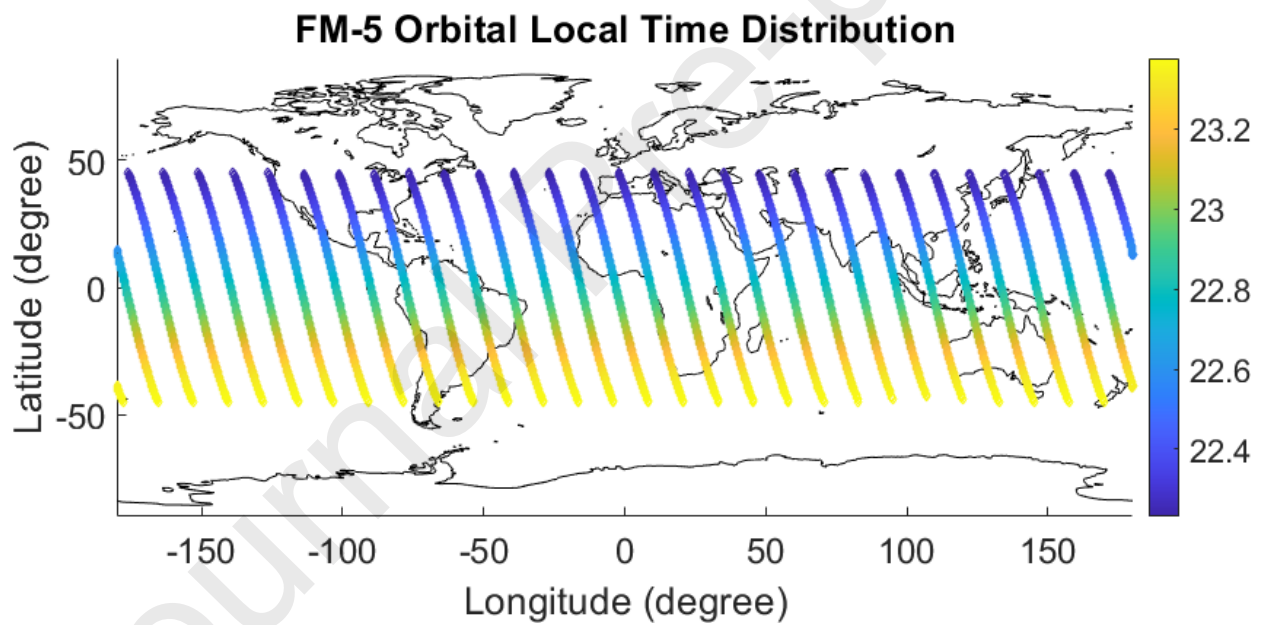


Figure 1: Locations of FORMOSAT-5 / AIP observations from October 2019 through October 2020, representative of the overall dataset. Local time is indicated by color.

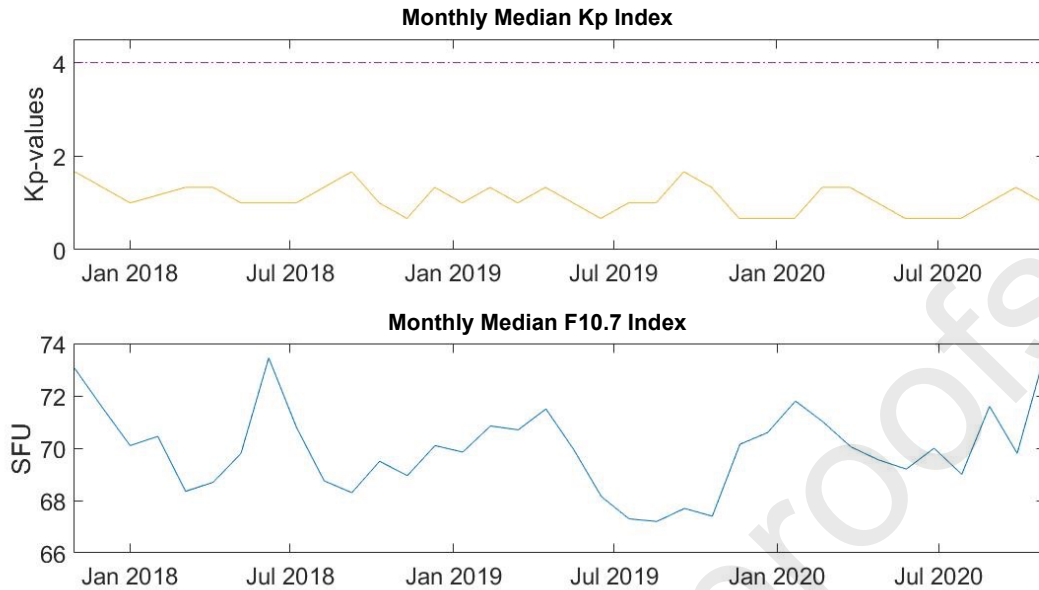


Figure 2: Monthly median Kp geomagnetic index (top) and monthly median F10.7 solar radio flux index (bottom) as a function of time from December 2017 through December 2020.

available via the National Aeronautics and Space Administration (NASA) Coordinated Data Analysis Web (CDAweb, https://cdaweb.gsfc.nasa.gov/misc/NotesF.html#FORMOSAT5_AIP_IDN) and the FORMOSAT-5 AIP Science Data Center (<http://sdc.ss.ncu.edu.tw/index.html>). FORMOSAT-5 was launched into a 720 km altitude and 98.28° inclination Sun synchronous orbit on August 25, 2017. This is a repeating orbit, with the spacecraft ground track passing over the same locations every two days, allowing for consistent geographic sampling. The local time of descending / ascending node for the FORMOSAT-5 orbit is at approximately 11:00 / 23:00. AIP has been operational on the ascending orbit of FORMOSAT-5 in the mid to low latitude region since mid-September 2017, typically equatorward of about 40° latitude with a sampling rate of 1 kHz, downsampled to 1 Hz in post-processing. The local times and geographic distribution of FORMOSAT-5/AIP observations are shown in Figure 1, which corresponds to the time period between October 2019 through October 2020. As expected, the locations of the in-situ measurements closely follow the ground track of FORMOSAT-5 in the low to mid latitudes, with local times in the range of 22:30 – 23:30, depending on latitude. The zonal spacing between adjacent orbits is approximately 10 degrees longitude.

For this study, we utilized FORMOSAT-5 / AIP ion density and vertical ion drift observations from December 2017 through December 2020. The temporal variation of the monthly median geophysical indices during this period of time is shown in Figure 2. From the variation of the median Kp geomagnetic index shown in the top panel of Figure 2, it can be seen that geomagnetic activity levels are low (less than 4) during the vast majority of this three-year period. The monthly median F10.7 solar radio flux (Figure 2, bottom) is low throughout this time period as well, with median values consistently in the range of 67 to 74 solar flux units (SFUs). The monthly median values exclude the effects of solar flares, which occasionally cause spikes in the range of 75 to 90 SFU. In general, the geomagnetic and solar activity levels are

representative of low solar activity conditions, indicating that baseline ionospheric parameters, such as plasma density and plasma drift, will show comparable values throughout this time (Choi et al., 2023).

The uncertainties of AIP observations are calculated based on the standard deviation of samples captured each second. This corresponds to 1024 samples for ion density and 256 samples for ion drift. The relative uncertainty in ion density is in the range of 3 to 10%, with the uncertainty being higher in regions of lower ion density. The absolute uncertainty in vertical ion drift is higher, in the range of 100 – 200 m s⁻¹. However, the coherent structures in the observations are still useful for identifying spatial variation and structure in vertical ion drift.

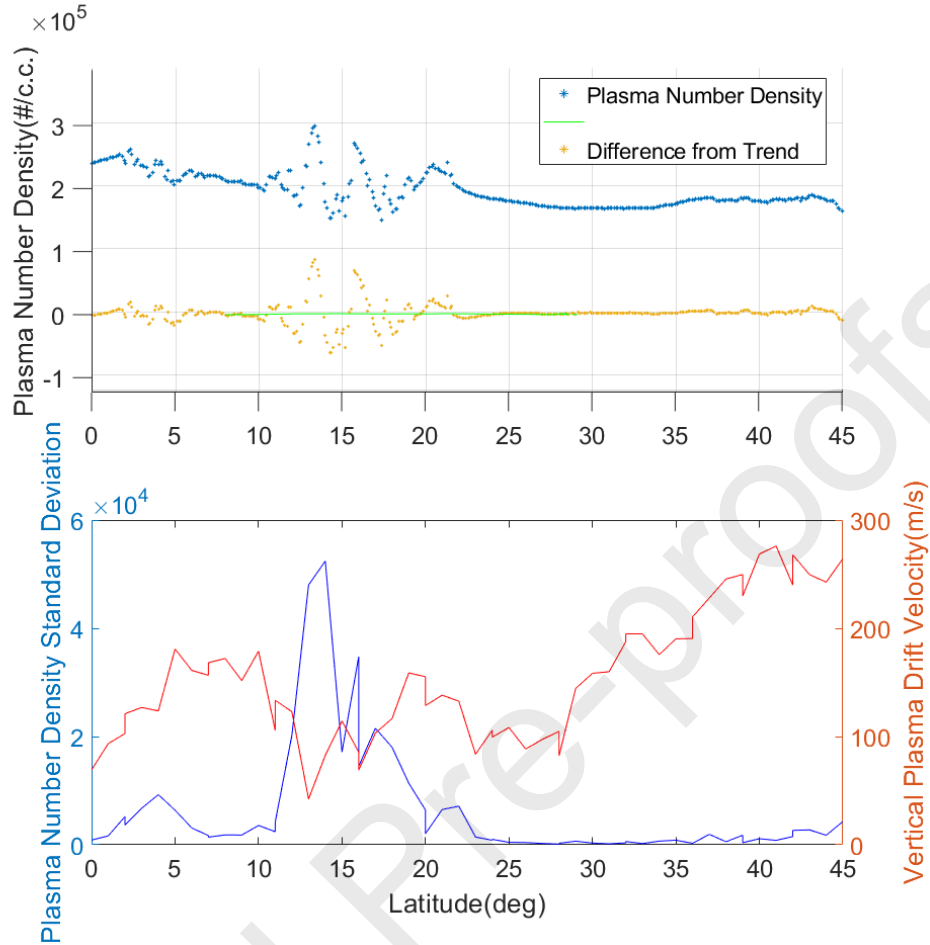


Figure 3: Top panel: latitude variation of raw ion densities observed by AIP during the ascending leg of a sample orbit on October 31, 2017 (blue dots), as well as de-trended ion densities from the same set of samples (yellow dots). Green line is baseline reference. Bottom panel: Standard deviation of de-trended ion densities from top panel, computed for 1° latitude bins (blue line); co-located vertical ion drift velocity with same binning (red line).

Ionospheric irregularities were routinely observed in AIP ion density measurements throughout the entire observation period of this study. An example of such irregularities can be seen in the top panel of Figure 3, which shows the raw ion density variation as a function of latitude observed by AIP during a sample orbit on January 26, 2018 as blue dots. Larger fluctuations with spatial scales less than 5° latitude can be seen between $0 - 7^\circ\text{N}$ and $10 - 22^\circ\text{N}$. Considering the location and spatial scale, these correspond to low latitude irregularities such as EPBs and MSTIDs. Since the FORMOSAT-5 orbital velocity of approximately 7.5 km s^{-1} is considerably larger than the range of phase velocities for MSTIDs and LSTIDs, these observations can be a snapshot of such TID irregularities. Similarly, the growth time of Rayleigh-Taylor instabilities that give rise to EPBs are on the order of tens of minutes, while EPBs themselves have a duration of 4 to 6 hours (Retterer, 2010). Combined with the 1 Hz sampling from AIP, as well as the spacecraft velocity, it can be assumed that the structure of EPBs observed in this manner are also relatively stationary snapshots.

To identify the occurrence and magnitude of these irregularities, we adapt a method similar to past studies, which have examined ionospheric irregularities using the depth of ion density depletions from a baseline background value (Huang et al., 2001), as well as the standard deviation of ionospheric parameters within a certain temporal or spatial interval (Sivakandan et al., 2021). We begin by de-trending the AIP ion densities to remove background values, which results in the yellow dots shown in the top panel of Figure 3. The standard deviation of this de-trended ion density profile (referred to hereafter as σ_N) is then calculated using 1° latitude bins and is shown in the bottom panel of Figure 3, along with the co-located vertical ion drift velocity measurements. Profiles for which there are fewer than five counts of data in a bin are discarded, which can result in some data gaps, especially during late 2017 and early 2018, when AIP was operated with a reduced duty cycle during spacecraft commissioning. To ensure consistency between the ion density and vertical ion drift velocity measurements, only orbital profiles where both measurements were available were used in this analysis. It can be seen by comparing the σ_N profiles with the raw ion density profiles that the former serves as a good indicator of the strength and occurrence locations of ion density irregularities and are utilized in the subsequent analysis to examine the spatial and temporal variability of ionospheric irregularities observed by FORMOSAT-5/AIP. Also considering the spatial scales of possible ionospheric irregularities, the de-trending and binning process also serves to suppress the signatures of LSTIDs. The irregularities identified in this study via σ_N therefore consist primarily of EPBs and MSTIDs.

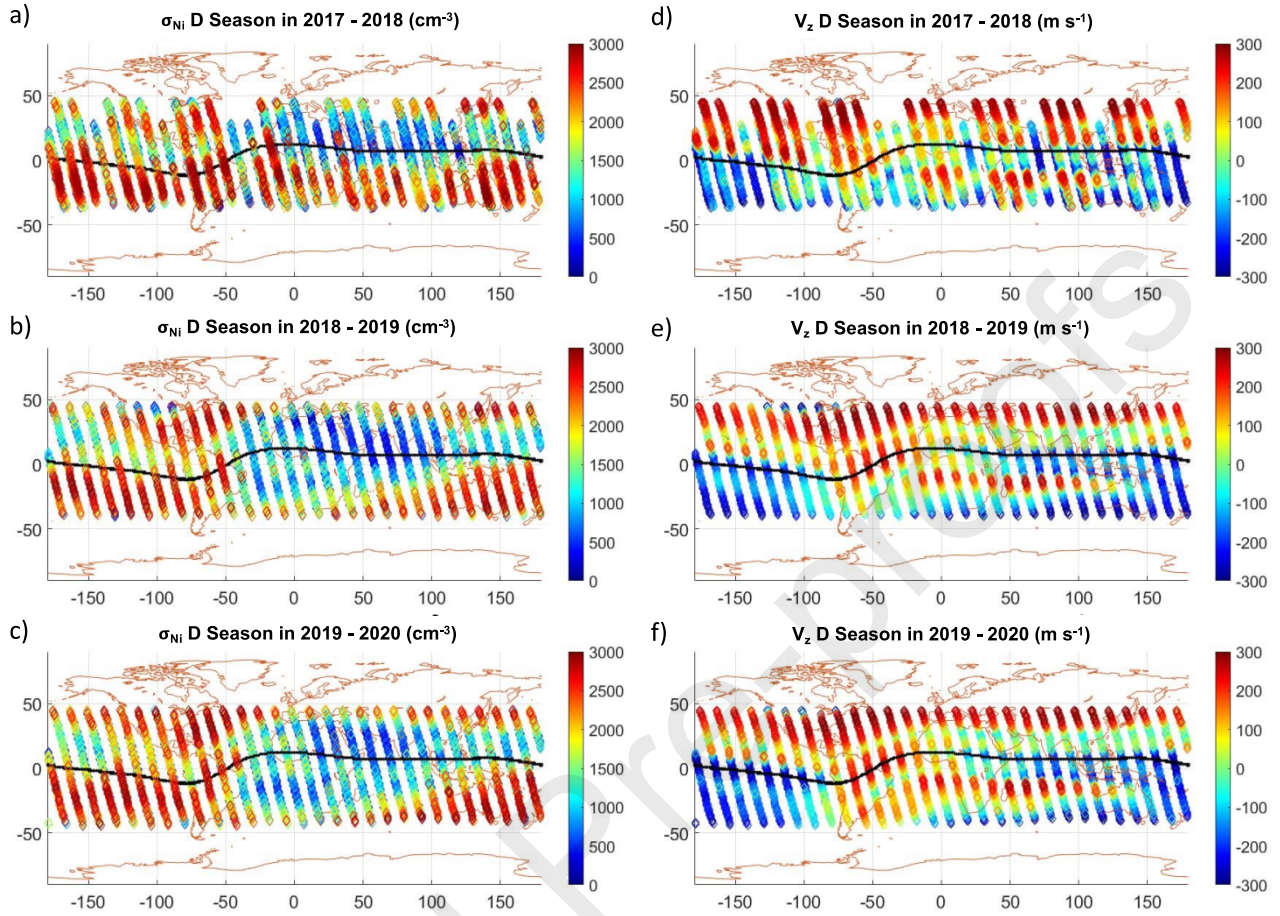


Figure 4: Left column: Distribution of ionospheric irregularities observed by FORMOSAT-5/AIP as represented by median σ_N during D season (boreal winter / austral summer). Right column: Distribution of median vertical ion drift observed by FORMOSAT-5/AIP during D season. Top row: 2017 – 2018, middle row: 2018 – 2019, bottom row: 2019 – 2020. Magnetic equator indicated by solid black line.

To identify the geographic variation of σ_N and vertical ion drift velocity (v_z) on a seasonal scale, we subdivide the annual data between December 2017 and December 2020 into four seasons: boreal winter / austral summer (referred to as “D season”, including November, December, January, and February), spring equinox (including March and April), austral winter / boreal summer (referred to as “J season”, including May, June, July, and August), and autumn equinox (including September and October). The σ_N and v_z values are binned into 1° latitude / longitude bins along the repeating orbit of FORMOSAT-5, and the median value of σ_N and v_z respectively calculated to serve as an indicator of the seasonal levels of ion density irregularities and vertical ion drift in the 22:30 – 23:30 local time (LT) sector.

3. Results

We first examine the distribution of ionospheric irregularities in the 22:30 – 23:30 LT sector as represented by FORMOSAT-5/AIP σ_N during D season, which corresponds to the boreal

winter / austral summer. The left column of Figure 4 shows the variation of the median value of σ_N along the FORMOSAT-5 nightside orbit during the D season of 2017 – 2018 (Figure 4a), 2018 – 2019 (Figure 4b), and 2019 – 2020 (Figure 4c). Certain features are common in the distribution of σ_N between the three years examined: large median values of σ_N , indicative of more irregularities, occur on either side of the magnetic equator around the EIA latitudes, as well as on the magnetic equator over South America. This is consistent with the known variation of EPBs, due to the larger vertical plasma gradients and background plasma densities in the regions about the EIA crests (Chou et al., 2020). The greater number of equatorial irregularities over the American sector is consistent with the higher occurrence of EPBs in this sector during the boreal winter due to the larger magnetic declination angle in this region (Tsunoda et al., 2015). Particularly large values of median σ_N are resolved during all three years in the mid latitudes extending across the EIA latitudes of Austronesia (approximately 100°E - 180°E), the Central Pacific Ocean (180°W - 120°W), and the Americas (120°W - 50°W). Significantly lower median values of σ_N , indicating a lower occurrence rate of ionospheric irregularities, are resolved in the lower and equatorial magnetic latitudes extending from over Africa (30°W) eastward to the Central Pacific (150°W). The lowest median values of σ_N in this quiet region occur following the magnetic equator over Africa, extending into Southeast Asia.

Despite the interannually recurrent features in the distribution of median σ_N and ionospheric irregularities during D seasons of the three years examined, there are still some features that demonstrate interannual variation. Compared to the median σ_N distribution in the D seasons of 2018 – 2019 and 2019 – 2020, the values of median σ_N during D season of 2017 – 2018 are generally larger, and especially so over the southern mid latitudes between the Atlantic Ocean and the Indian Ocean. This indicates that the interannually recurrent D season quiet region was significantly smaller during this first year of observations compared to the two latter years. It can thus be concluded that geographic distribution and magnitude of ionospheric irregularities observed by FORMOSAT-5/AIP during the D season of 2017 – 2018 differed considerably compared to the two latter years. Although the maximum monthly median F10.7 index varied by only about 3 SFUs during the three D seasons examined, it should be noted that solar minimum occurred in December 2019, which could explain the interannual variability observed (National Weather Service, 2020).

We now consider the 22:30 – 23:30 LT vertical ion drift velocity (v_z) observed by FORMOSAT-5/AIP, which are shown in the right column of Figure 4. These values correspond to the D seasons of 2017 – 2018 (Figure 4d), 2018 – 2019 (Figure 4e), and 2019 – 2020 (Figure 4f). Positive values of v_z in the post sunset ionosphere are correlated with the occurrence of EPBs, albeit usually at an earlier local time than the range sampled by FORMOSAT-5/AIP (Smith et al., 2016; Su et al., 2008; Chou et al., 2020). From these figures, there are again some interannually recurrent features in the positive v_z distribution during the three years examined. Latitudinal enhancements in positive v_z occur in the mid latitudes on both sides of the magnetic equator, as well as on the magnetic equator. There is however a strong hemispheric asymmetry, with the positive v_z in the northern hemisphere enhancement region being much larger than those in the southern hemisphere and over the equator. The longitudinal variation of these three enhancement regions also varies considerably, with the northern v_z enhancement being very zonally broad, extending across all longitudes observed. On the other hand, the interannually

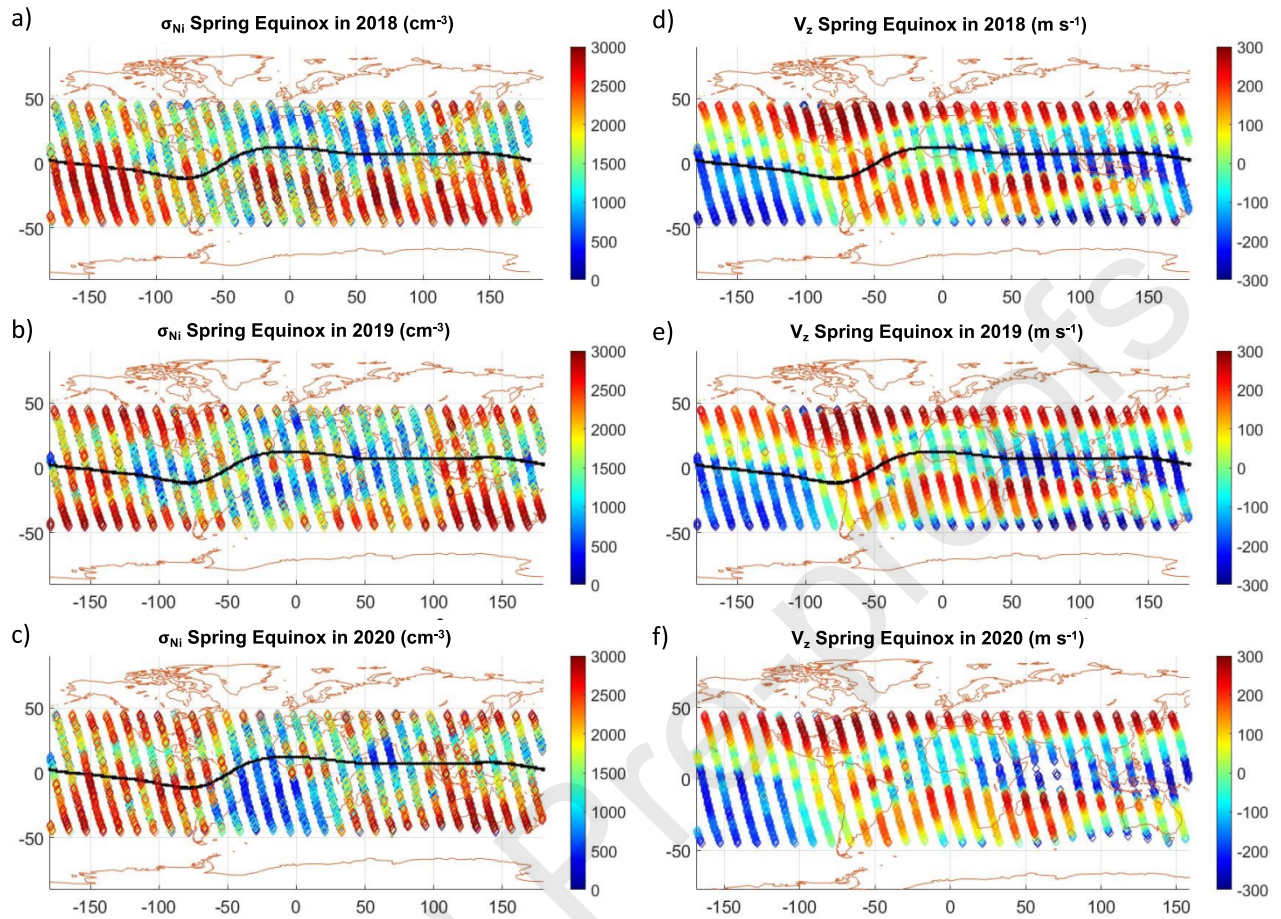


Figure 5: Left column: Distribution of ionospheric irregularities observed by FORMOSAT-5/AIP as represented by median σ_N during spring equinox). Right column: Distribution of median vertical ion drift observed by FORMOSAT-5/AIP during spring equinox. Top row: 2018, middle row: 2019, bottom row: 2020. Magnetic equator indicated by solid black line.

recurrent equatorial enhancement is limited mainly to the American sector with a thinner extension just north of the magnetic equator stretching towards the Central Pacific and Africa. The southern enhancement in positive v_z is somewhat broader zonally than the equatorial enhancement extending from the South Atlantic to Australia. Although there are some interannual differences in v_z between the three years examined, the level of interannual consistency is considerably higher with v_z compared to with σ_N . The most prominent features of interannual variation are the larger values of positive v_z during the D season of 2017 – 2018 compared to the two latter years, particularly in the northern hemisphere enhancement, as well as the location of the equatorial enhancement, with the largest values of v_z shifted westward toward the Eastern and Central Pacific.

We now examine the variation of ionospheric irregularities and v_z during spring equinox. The left column of Figure 5 corresponds to the median values of σ_N during the spring equinoxes of 2018 (Figure 5a), 2019 (Figure 5b), and 2020 (Figure 5c). Examining the latitudes on and immediately adjacent to the magnetic equator, it can be seen that the geographic distribution of

these equatorial irregularity enhancements is concentrated around a few distinct regions, including the Central Pacific, Africa, as well as East Asia, forming a “wave-3” zonal variation. Equatorial enhancements in irregularities are also observed extending over South America in 2020. Polewards of the magnetic equator and towards the two EIA regions and the mid latitudes, the values of σ_N in the southern hemisphere are generally larger than those observed in the northern hemisphere, although this could be an artifact of the northward bias of the magnetic equator in the latitudinal span observed. The southern hemisphere enhancements in σ_N are strongest in a zonal region spanning from the Indian Ocean eastward to South America, with a quiet region over the Southern Atlantic region in 2019 and 2020. This quiet region is not observed in 2018, which shows a higher median σ_N in this region and by extension, a larger number of irregularities.

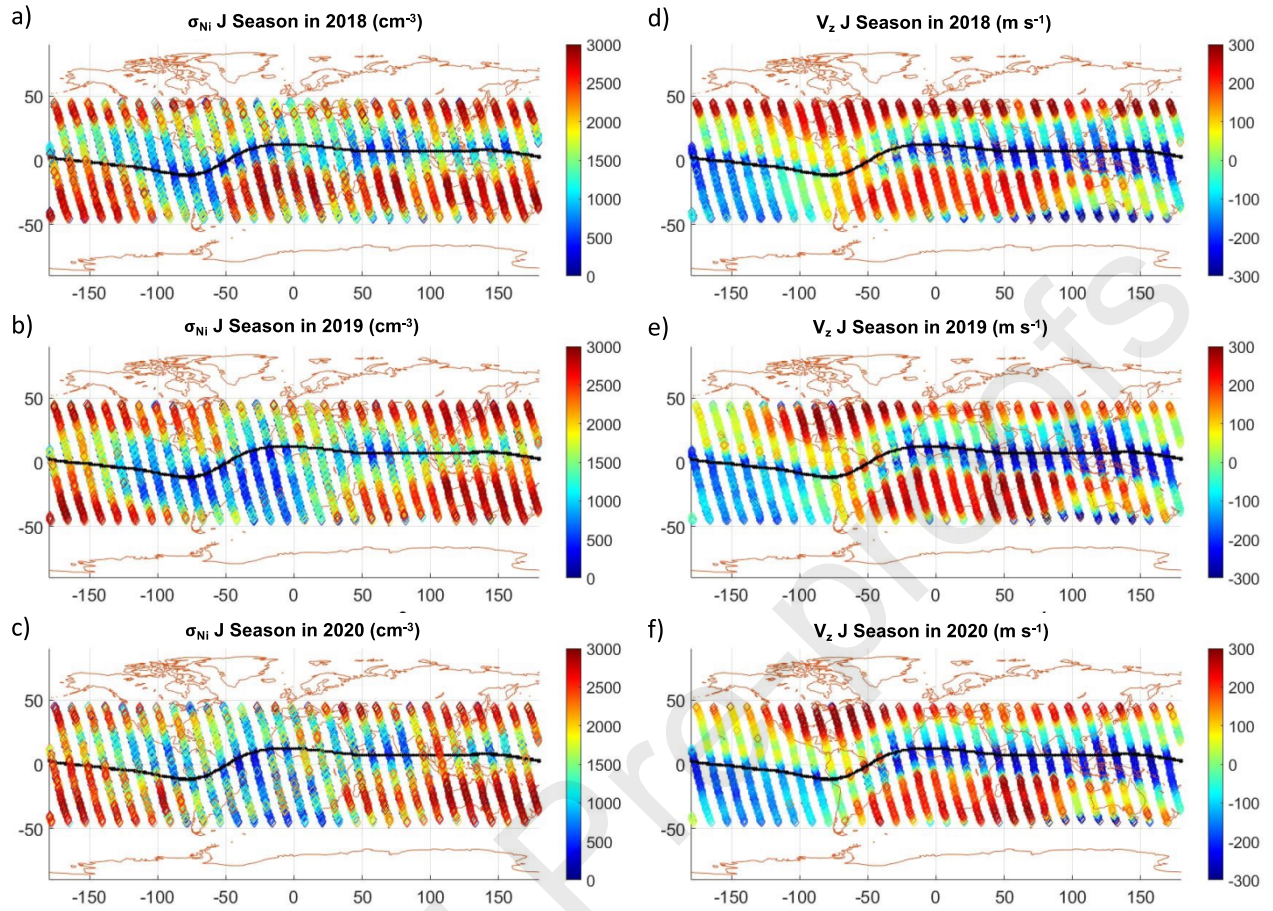


Figure 6: Same as Figure 5, but for J season (boreal summer / austral winter).

The spring equinox v_z observed by FORMOSAT-5/AIP are shown in the left column of Figure 5. The spatial distribution of the vertical ion drift velocities show many similarities to those of D season (Figure 5, right column): an equatorial enhancement in positive v_z is resolved about the magnetic equator centered over South America, extending zonally in both directions slightly biased to the north side of the magnetic equator. Enhancements in positive v_z are also resolved off of the magnetic equator near the EIA latitudes of both hemispheres, with the visible portion of the northern enhancement over North America and that in the southern hemisphere EIA latitudes extending zonally in a broad region extending from the South Atlantic to Australia. Compared to D season, the positive v_z are larger in magnitude by approximately 100 m s^{-1} in the magnetic equatorial and southern hemisphere enhancements, showing the beginning signs of a hemispherical shift in positive v_z towards the southern hemisphere. Another prominent difference between D season in 2017 - 2018 and spring equinox in 2018 is that the positive v_z extending from the Middle East to East Asia is weaker in the latter compared to the former. Compared to D season however, the level of interannual variability in vertical ion drift during spring equinox is considerably lower during the three years examined.

Figure 6 shows FORMOSAT-5/AIP results for J season, which corresponds to boreal summer and austral winter. Similar to Figure 5, the left column shows the median values of σ_N

during the J seasons of 2018 (Figure 6a), 2019 (Figure 6b), and 2020 (Figure 6c). Compared to the boreal winter / austral summer D season results shown in the left column of Figure 4, one immediately apparent difference is the change in geographic location of the quiet regions with lower median values of σ_N . The quiet region in D season existed as a large continuous patch extending from the African to the East Asian and Central Pacific sectors. In J season, four distinct patches with lower median σ_N are observed over the Eastern Pacific, the Atlantic Ocean, the Indian Ocean, and East Asia. It is notable that an additional quiet patch in the southern hemisphere off of the magnetic equator is observed over the South Atlantic and Southern Africa in the J seasons of 2019 (Figure 6b) and 2020 (Figure 6c), but not in 2018 (Figure 6a). This indicates a higher occurrence rate of irregularities observed over this region during the first year of observations, compared to the latter two years.

Similar to D season, the regions of higher median σ_N in J season, indicative of more irregularities, are observed on either side of the magnetic equator at the mid latitudes. Unlike the D season results, the regions where larger median σ_N are observed in J season show more distinct zonal modulation. In all three years, regional peaks in median σ_N are observed in the southern hemisphere over the Indian Ocean, Austronesia, and the Central Pacific. An additional regional peak in median σ_N is observed in 2018 off the coast of Western Africa, forming a “wave-4” pattern, whereas the zonal variability in the two other years is more characteristic of “wave-3”. Zonal modulation of median σ_N is less observable due to the northward bias of the magnetic equator in the FORMOSAT-5/AIP dataset, although regional peaks are observed over East Asia and the Central Pacific. Although the largest values of median σ_N during J season are located around the mid latitudes, smaller equatorial peaks in median σ_N are still observed, occurring around Northern Africa (2019 and 2020), Southeast Asia (all three years, but particularly strong in 2020), and the Central Pacific (particularly strong in 2019 and 2020).

The v_z observed by FORMOSAT-5/AIP during J season is shown in the right column of Figure 6. The spatial variation of the v_z during J season again echoes those of the two previously shown seasons showing northern and southern hemisphere mid latitude peaks of positive v_z , as well as a narrower equatorial peak. The hemispheric variation has also changed, with stronger positive v_z now observed in the southern mid latitude region. Nonetheless, the relative difference between the northern and southern mid latitude peaks in positive v_z are smaller in J season compared to D season. The zonal extent of the equatorial peak in positive v_z is also smaller in J season compared to the two other seasons previously examined. Nonetheless, the equatorial peak is still located over South America. The level of interannual variation in v_z observed during J season is again much less than that observed in median σ_N . The most prominent interannual difference is that the northern hemisphere peak in positive v_z is larger in magnitude in 2018 (Figure 6d), even exceeding the values observed in the southern hemisphere peak. The maximum values of the northern and southern hemisphere peaks during the J seasons of 2019 and 2020 were much more comparable in magnitude.

The left column of Figure 7 shows the median σ_N observed during the autumn equinox. Distinct regions of median σ_N enhancements along the magnetic equator are observed over the Central Pacific, South America, Africa (considerably stronger in 2020), and Southeast Asia

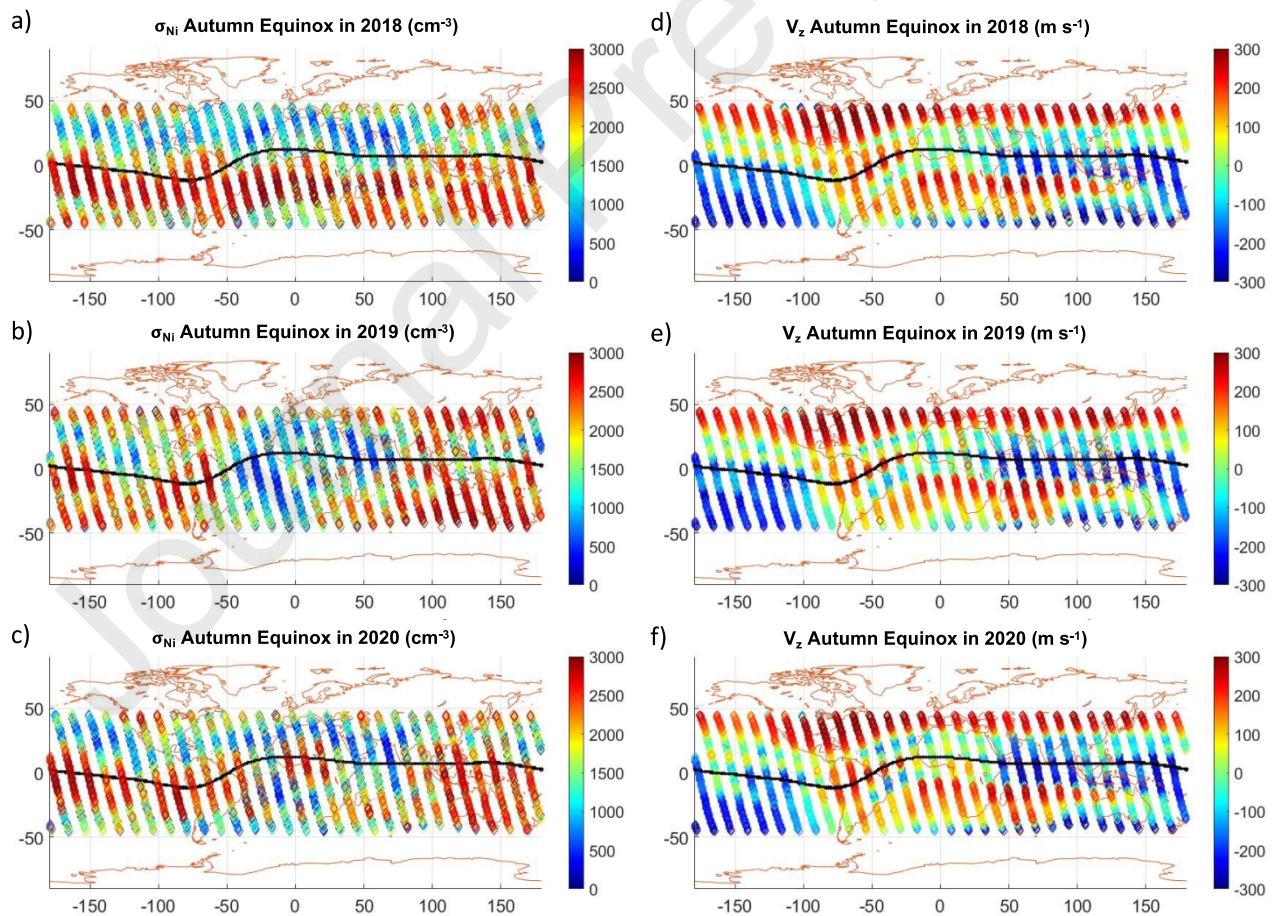


Figure 7: Same as Figure 5, but for autumn equinox.

forming a “wave-4” zonal modulation. Enhancements of median σ_N off of the magnetic equator are also resolved around the mid latitudes of both hemispheres, with the more prominent southern mid latitude enhancement being considerably stronger and zonally broader in 2018 compared to the two latter years. A “wave-4” zonal modulation of the southern EIA enhancement of median σ_N is observed to be particularly prominent in 2018, with peaks located over the Central Pacific, the South Atlantic, the Indian Ocean, and Austronesia. Like the three other seasons previously examined, the median σ_N over the South Atlantic is much lower in 2019 and 2020, indicative of a lower occurrence of ionospheric irregularities in this region during these two latter years, making the “wave-4” less immediately apparent.

The vertical ion drift velocities for autumn equinox are shown in the right column of Figure 7. The overall geographic distribution of v_z has not changed significantly compared to the three other seasons and is relatively consistent for all three years examined. Compared to J season, the enhancements in positive v_z in the southern mid latitudes have decreased in magnitude, while the equatorial and northern mid latitude positive v_z enhancements have increased in magnitude. We may therefore conclude that compared to the distribution of median σ_N , the geographic distribution of v_z observed by FORMOSAT-5/AIP shows relatively little interannual variation, with a regular seasonal variation that sees strengthened enhancements of v_z in the mid latitudes of the winter hemisphere.

4. Discussion

From the FORMOSAT-5/AIP observations, we have resolved a few key features of the recurring spatial and seasonal variation in the observed median σ_N , corresponding to the occurrence of ionospheric irregularities, as well as v_z . It is important to note that both datasets correspond to in-situ observations between 22:30 – 23:30 LT at 720 km altitude, which corresponds to the topside ionosphere well above the F-region peak (Zou et al., 2000).

Table 1: Zonal median σ_N along magnetic latitudes of 15°S, 0°, and 15°N during D season (D), Spring equinox (Sp), J season (J), and Autumn equinox (Au) during 2018, 2019, and 2020. Units of cm^{-3} . Note that D season also includes November and December of the prior year.

Year	15°S				0°				15°N			
	D	Sp	J	Au	D	Sp	J	Au	D	Sp	J	Au
2018	1381	957	1307	1064	980	641	600	841	790	502	982	477
2019	1003	759	881	725	719	563	433	584	784	655	883	569

2020	904	697	1166	704	633	576	728	989	808	607	905	478
------	-----	-----	------	-----	-----	-----	-----	-----	-----	-----	-----	-----

Enhancements in median σ_N can generally be grouped into those occurring along the magnetic equator, as well as those occurring near the mid latitudes of both hemispheres. Table 1 is a tabulation of the seasonal and interannual variation of the zonal median σ_N along 15°S, 0°, and 15°N magnetic latitude. At 15°S and 15°N, median σ_N consistently shows a semiannual variation with the largest median values occurring during the solstice seasons. At the magnetic equator, the variation is annual in nature. Of the four seasons at 15°S, median σ_N showed a monotonic decrease over the three years examined. At the two other magnetic latitudes, median σ_N decreased between 2018 to 2019 in six of the eight sample locations.

It is notable that a large region with low levels of median σ_N is observed in the low and equatorial latitudes, which can extend from the Atlantic to the Western Pacific in the D season, as well as in more localized patches during other seasons. Distinct enhancements in median σ_N centered about the magnetic equator are more commonly observed during the equinoxes (both spring and autumn), while equatorial enhancements in median σ_N during the solstices, especially D season, tend to blend in with enhancements extending from the mid latitudes. The overall seasonal variability of these equatorial irregularities observed by FORMOSAT-5/AIP is consistent with the known climatology of EPBs, notably the enhancement in irregularities over the American sector during the D season, the enhancements over the Central Pacific and African sectors during the J season, as well as the more widespread distribution of equatorial irregularities during the spring and autumn equinoxes (Gentile et al., 2006). This seasonal variation has been primarily attributed to vertical plasma drift being largest when the solar terminator aligns with magnetic field lines, which tends to be around the equinoxes for sectors with small magnetic declination angles and during boreal winter in the American sector due to the larger magnetic declination angle there. On the other hand, the boreal summer increase in EPB occurrence in the Central Pacific and African sectors has been attributed to modulation of vertical plasma drift by nonmigrating atmospheric tides. As vertical plasma drift contributes the positive vertical plasma gradient that favors EPB formation, nighttime vertical plasma drift exceeding a threshold value is considered a necessary through not sufficient condition for EPB formation (Tsunoda et al., 2015; Chang et al., 2021). We therefore surmise that these equatorial enhancements in median σ_N correspond predominately to the presence of EPBs.

It is notable that the zonal variation of these equatorial enhancements shows a distinct “wave-3” pattern during spring equinox (Figure 5, left) and a “wave-4” pattern during autumn equinox (Figure 7, left), which respectively coincide with the known variation of the nonmigrating diurnal tide with eastward zonal wavenumber 2 (DE2) and eastward zonal wavenumber 3 (DE3). DE2 is known to maximize from March through June, while DE3 maximizes from August through October (Chang et al., 2013). Evidence for tidal modulation of these EPB signatures is further strengthened in that the longitudes of these equatorial “wave-3” and “wave-4” enhancements in median σ_N closely match those observed in FORMOSAT-3/COSMIC TEC. Despite corresponding to observations between 2007 – 2011, the longitudes of the TEC “wave-

3” and “wave-4” were found to be quite consistent from year to year (Chang et al., 2013). These “wave-3” and “wave-4” patterns in irregularities can be further modulated as was seen in the autumn equinox of 2019 due to the relatively smaller values of the enhancement in irregularities over Africa (Figure 7b).

Away from the magnetic equator, a significant portion of the median σ_N enhancements detected by FORMOSAT-5/AIP were distributed near the mid latitudes of both hemispheres, also demonstrating systematic aspects of seasonal and interannual variation. Although present during all of the seasons examined, these mid latitude enhancements in irregularities showed much more zonal variability in 2019 and 2020 compared to 2018. More of these southern mid latitude irregularities were observed over the South Atlantic and Southern Africa in 2018, compared to the two latter years. As mentioned previously, this might be due to the solar minimum occurring in December 2019 (National Weather Service, 2020). As a result, the first year might show more residual effects from periods of higher solar activity. The seasonal and longitudinal variation of these mid latitude irregularities bears less resemblance to the variation of EPBs mentioned previously and may therefore include contribution from other sources of ionospheric irregularities of this scale such as MSTIDs. It is notable that since EPBs extend along magnetic field lines, at the higher 720 km orbit of FORMOSAT-5, we would expect more EPB signatures near the magnetic equator, with off-equator EPB signatures being more prominent at lower altitudes. In past studies using in situ observations, the vast majority of EPBs detected by the Defense Meteorological Satellite Program (DMSP) satellites at 848 km altitude and ROCSAT (now known as FORMOSAT-1) at 650 km altitude were detected within 20° of the equator (Burke et al., 2004), further indicating that these mid latitude irregularities observed by FORMOSAT-5/AIP consist of phenomena other than EPBs.

Because of the limited continuous coverage of FORMOSAT-5/AIP at mid latitudes, beyond the higher occurrence rate of such mid latitude irregularities over the South Atlantic in 2018 compared to 2019 and 2020, it is difficult to resolve the seasonal variation of irregularities in this region, especially during spring equinoxes of all three years and the D season of 2017 - 2018. Due to their similar spatial coverage, a limited amount of seasonal variability can be identified by comparing the median σ_N observations between the J seasons (Figure 6) and autumn equinoxes (Figure 7) of the three years examined. It can be seen from the two figures that the values of mid latitude median σ_N are larger during the J season solstice compared to the autumn equinox conditions over the northern mid latitudes in general, as well as the Southern Central Pacific for all three years examined. Differences between the two seasons in other regions are much more variable from year to year, with the magnitudes of J season median σ_N being larger than autumn equinox over Australia in 2018 and 2020 (panels a and c of Figure 6 and Figure 7), but comparable in 2019 (panel b of Figure 6 and Figure 7).

There have been considerably fewer studies on the interannual variability of ionospheric irregularities compared to studies on seasonal and local time variability. One multi-year study on the characteristics of EPBs observed by the Communication/Navigation Outage Forecasting System (C/NOFS) satellite from 2008 to 2014 did report inter-annual variability in the local time of highest occurrence probability, with EPBs occurring preferentially in the postmidnight sector during times of low solar activity, while there was relatively little interannual change in EPB width (Smith and Heelis, 2017). Given the FORMOSAT-5/AIP sampling in the pre-midnight

sector, decreases in irregularities resolved during the three years examined could therefore be attributed to declining solar activity.

Although considerable seasonal and interannual variability was observed in median σ_N and by extension, the occurrence of ionospheric irregularities, considerably less variability at these temporal scales was resolved in the v_z observed by FORMOSAT-5/AIP. A large post sunset vertical ion drift has long been identified as a necessary but not sufficient condition for EPB formation and correlated to larger Rayleigh-Taylor growth rates and EPB occurrence rates (Smith et al., 2016). The relation between median σ_N and v_z about the magnetic equator over South America during J season (Figure 6) and autumn equinox (Figure 7) is consistent with this hypothesis. It can be seen from the left columns of both Figures that median σ_N along the magnetic equator over South America is significantly larger during autumn equinox compared to J season. Similarly, v_z (right columns of Figure 6 and Figure 7) over the same magnetic equatorial region above South America are also larger in magnitude and broader in spatial extent in autumn equinox compared to J season. A similar situation exists for the African sector along the magnetic equator where larger values of median σ_N during autumn equinox compared to J season in 2018 and 2020 were correlated with a similar relation in v_z . However, it is notable that with the exception of the two aforementioned examples, it is difficult to find a direct resemblance between the geographic distribution and seasonal variation of the enhancements in median σ_N and v_z at other seasons and locations. This could be attributed to a few different reasons. First, the observations shown correspond to the local time zone between 22:30 – 23:30, due to the orbit of FORMOSAT-5 and the duty cycle of the AIP payload. This corresponds to a much later local time sector in the post-sunset ionosphere compared to the 18 – 19 LT vertical drifts of the PRE responsible for ionospheric uplift (Su, et al., 2008), as well as the 18 – 19 LT EPB growth phase (Chou et al., 2020). Second, the mid latitude irregularities are likely to be attributable to phenomena other than EPBs, such as nighttime MSTIDs, which are produced by other driving mechanisms.

The above results demonstrate the capabilities of FORMOSAT-5/AIP in observing ionospheric irregularities, as well as ionospheric parameters such as vertical ion drift velocity that are a driver for the formation of EPBs. The observational limitations in terms of local time and latitude caused by a single satellite platform in a Sun-synchronous orbit reflect the need for multiple satellite platforms with in-situ instruments, which will greatly enhance observational capacity (Duann et al., 2020; Chandran et al., 2021). This can be made possible with the growing maturity and reduced cost of small satellites, as well as the growth of international small satellite initiatives (Millan et al., 2019; Baker et al., 2020).

Conclusions

In this study, we have examined the geographic, seasonal, and interannual variability of ionospheric irregularities and vertical ion drift velocities observed by FORMOSAT-5/AIP during the low solar activity conditions from 2017 - 2020. The results correspond to in-situ observations along the FORMOSAT-5 satellite orbit at 720 km and local times between 22:30 – 23:30. Consistent patterns of geographic and seasonal variability are observed, especially in the case of

vertical ion drift velocities. Magnetic equatorial and low latitude irregularities show distinctive longitudinal and seasonal variability consistent with those of EPBs, while also showing signs of modulation by nonmigrating tides during the spring and autumn equinoxes. Mid-latitude irregularities are also present but show less consistency with the expected variation of EPBs and may correspond to MSTIDs. Significant signs of interannual variability observed include a much higher occurrence rate of mid latitude irregularities over the South Atlantic and Southern Africa in 2017 - 2018 compared to 2019 and 2020. The results can be further extended through the deployment of similar in-situ instruments aboard multiple satellite platforms, a possibility becoming more feasible with the growing maturity and proliferation of small satellites.

Acknowledgements

The FORMOSAT-5 / AIP ion density and vertical ion drift data utilized in this study are available via the National Aeronautics and Space Administration (NASA) Coordinated Data Analysis Web (CDAweb, https://cdaweb.gsfc.nasa.gov/misc/NotesF.html#FORMOSAT5_AIP_IDN) and the FORMOSAT-5 AIP Science Data Center (<http://sdc.ss.ncu.edu.tw/index.html>). The F10.7 solar radio fluxes were obtained from the LASP Interactive Solar Irradiance Data Center (https://lasp.colorado.edu/lisird/data/penticton_radio_flux/), while the Kp geomagnetic indices were obtained from the NOAA National Centers for Environmental Information (https://www.ngdc.noaa.gov/stp/geomag/kp_ap.html). This research was funded by grants 110-2923-M-008-005-MY3, 111-2636-M-008-004, and 112-2636-M-008-003 from the Taiwan National Science and Technology Council to L.C. Chang, grant NSTC 112-2923-M-008-005 to J.-Y. Liu, as well as the Higher Education SPROUT grant from the Taiwan Ministry of Education to the National Central University Center for Astronautical Physics and Engineering.

References

Baker, D., Chandran, A., Chang, L., Macdonald, M., Meftah, M., Millan, R.M., Park, J.U., Praveen Kumar, K., Price, C., von Steiger, R. & Wu, J., 2020. An International Constellation of Small Spacecraft. *Space Research Today*, August, Volume 208, pp. 23 - 28.

Batista, I. S., Abdu, M. A. & Bittencourt, J. A., 1986. Equatorial F region vertical plasma drift: Seasonal and longitudinal asymmetries in the American sector. *Journal of Geophysical Research*, Volume 91, pp. 12,055 - 12,064.

Burke, W. J., Gentile, L. C., Huang, C. Y., Valladares, C. E. & Su, S. Y., 2004. Longitudinal variability of equatorial plasma bubbles observed by DMSP and ROCSAT-1. *Journal of Geophysical Research*, Volume 109, A12301, doi:10.1029/2004JA010583.

Chandran, A., Fang, T-W., Chang, L., Priyadarshan, H., Woods, T.N., Chao, C-K., Kohnert, R., Verma, A., Boyajian, S., Duann, Y., Evonosky, W., Kompella, M., Tsai-Lin, R., Kumar, A., Srivastava, S., Schwab, B., Sewell, R. & Sarpotdar, M., 2021. The INSPIRESat-1: Mission, Science, and Engineering. *Advances in Space Research*, Volume 68, pp. 2616 - 2630, <https://doi.org/10.1016/j.asr.2021.06.025>.

Chang, L.C., Lin, C.-H., Yue, J., Liu, J.-Y. & Lin, J.-T., 2013. Stationary planetary wave and nonmigrating tidal signatures in ionospheric wave 3 and wave 4 variations in 2007–2011 FORMOSAT-3/COSMIC observations. *Journal of Geophysical Research Space Physics*, 118(10), pp. 6651 - 6665, <https://doi.org/10.1002/jgra.50583>.

Chang, L. C., Salinas, C.C.J.H., Chiu, Y.-C., Jones Jr, M., Rajesh, P. K., Chao, C.-K., Liu, J.-Y., Lin, C.C.H. & Hsiao, T.-Y., 2021. Implication of tidal forcing effects on the zonal variation of solstice equatorial plasma bubbles. *Journal of Geophysical Research Space Physics*, Volume 126, e2020JA028295, <https://doi.org/10.1029/2020JA028295>.

Chao, C.-K., Su, S.-Y. & Liu, C. H., 2020. Initial nighttime ionospheric observations with advanced ionospheric probe onboard FORMOSAT-5. *Advances in Space Research*, Volume 65, pp. 2405 - 2411, <https://doi.org/10.1016/j.asr.2020.02.009>.

Chen, G., Zhou, C., Liu, Y., Zhao, J., Tang, Q., Wang, X. & Zhao, Z., 2019. A statistical analysis of medium-scale traveling ionospheric disturbances during 2014-2017 using the Hong Kong CORS network. *Earth Planets Space*, 71(1), 52, <https://doi.org/10.1186/s40623-019-1031-9>.

Choi, J.-M., Lin, C.C.-H., Rajesh, P.K., Park, J., Kwak, Y.-S., Chen, S.-P., Lin, J.-T. & Chang, M.-T., 2023. Comparisons of in situ ionospheric density using ion velocity meters onboard FORMOSAT-7/COSMIC-2 and ICON missions. *Earth, Planets and Space*, Volume 75, 15, <https://doi.org/10.1186/s40623-022-01759-3>.

Chou, M.-Y., Wu, Q., Pedatella, N. M., Cherniak, I, Schreiner, W.S. & Braun, J., 2020. Climatology of the Equatorial Plasma Bubbles Captured by FORMOSAT-3/COSMIC. *Journal of Geophysical Research Space Physics*, Volume 125, e2019JA027680, <https://doi.org/10.1029/2019JA027680>.

Duann, Y., Chang, L.C., Chao, C.-K., Chiu, Y.-C., Tsai-Lin, R., Tai, T.-Y., Luo, W.-H., Liao, C.-T., Liu, H.-T., Chung, C.-J., Duann, R., Kuo, C.-L., Liu, J.-Y., Yang, Z.-M., Gacal, G.F., Chandran, A., Priyadarshan H., Verma, A., Fang, T.-W. & Sarthak S., 2020. IDEASSat: A 3U CubeSat mission for ionospheric science. *Advances in Space Research*, Volume 66, pp. 116 - 134, <https://doi.org/10.1016/j.asr.2020.01.012>.

Fesen, C. G., Crowley, G., Roble, R. G., Richmond, A. D. & Fejer, B. G., 2000. Simulation of the pre-reversal enhancement in the low latitude vertical ion drifts. *Geophysical Research Letters*, Volume 27, pp. 1851 - 1854, <https://doi.org/10.1029/2000GL000061>.

Gardner, L. C. & Schunk, R. W., 2010. Generation of traveling atmospheric disturbances during pulsating geomagnetic storms. *Journal of Geophysical Research*, Volume 115, A08314, <https://doi.org/10.1029/2009JA015129>.

Gentile, L. C., Burke, W. J. & Rich, F. J., 2006. A global climatology for equatorial plasma bubbles in the topside ionosphere. *Annales Geophysicae*, Volume 24, pp. 163 - 172.

Hocke, K. & Schlegel, K., 1996. A review of atmospheric gravity waves and travelling ionospheric disturbances: 1982-1995. *Annales Geophysicae*, 14(9), pp. 917 - 940.

Huang, C. Y., Burke, W. J., Machuzak, J. S., Gentile, L. C. & Sultan, P. J., 2001. DMSP observations of equatorial plasma bubbles in the topside ionosphere near solar maximum. *Journal of Geophysical Research*, Volume 106, pp. 8131 - 8142, <https://doi.org/10.1029/2000JA000319>.

International Telecommunication Union, 2017. *Recommendation ITU-R P.618-13 (12/2017) Propagation data and prediction methods required for the design of Earth-space telecommunication systems*. [Online] Available at: https://www.itu.int/dms_pubrec/itu-r/rec/p/R-REC-P.618-13-201712-I!!PDF-E.pdf [Accessed 30 January 2023].

International Telecommunication Union, 2019. *Recommendation ITU-R P.531-14 Ionospheric propagation data and prediction methods required for the design of satellite networks and*

systems. [Online] Available at: https://www.itu.int/dms_pubrec/itu-r/rec/p/R-REC-P.531-14-201908-I!!PDF-E.pdf [Accessed 11 January 2023].

Kil, H., 2015. The Morphology of Equatorial Plasma Bubbles - a review. *Journal of Astronomy and Space Sciences*, 32(1), pp. 13 - 19, <https://doi.org/10.5140/JASS.2015.32.1.13>.

Lin, Z.-W., Chao, C. K., Liu, J. Y., Huang, C. M., Chu, Y. H., Su, C. L., Mao, Y. C. & Chang, Y. S., 2017. Advanced Ionospheric Probe scientific mission onboard FORMOSAT-5 satellite. *Terrestrial Atmospheric and Oceanic Sciences*, 28(2), pp. 99 – 110, <https://doi.org/10.3319/TAO.2016.09.14.01> (EOF5).

Liu, Y., Zhou, C., Xu, T., Tang, Q., Deng, Z. X., Chen, G. Y. & Wang, Z. K. , 2021. Review of ionospheric irregularities and ionospheric electrodynamic coupling in the middle latitude region. *Earth and Planetary Physics*, 5(5), pp. 462 - 482, <http://doi.org/10.26464/epp2021025>.

Makela, J. & Otsuka, Y., 2012. Overview of Nighttime Ionospheric Instabilities at Low- and Mid-Latitudes: Coupling Aspects Resulting in Structuring at the Mesoscale. *Space Science Reviews*, Volume 168, pp. 419 - 440, DOI 10.1007/s11214-011-9816-6.

Merlino, R. L., 2007. Understanding Langmuir probe current-voltage characteristics. *American Journal of Physics*, 75(1078), pp. 1078 – 1085, <https://doi.org/10.1119/1.2772282>.

Millan, R., von Steiger, R., Ariel, M., Bartalev, S., Borgeaud, M., Campagnola, S., Castillo-Rogez, J.C., Fléron, R., Gassi, V., Gregorio, A., Klumpar, D.M., Lal, B., Macdonald, M., Park, J.U., Rao, V.S., Schilling, K., Stephens, G., Title, A.M. & Wu, J., 2019. Small satellites for space science A COSPAR scientific roadmap. *Advances in Space Research*, Volume 64, pp. 1466 – 1577, <https://doi.org/10.1016/j.asr.2019.07.035>.

NASA Small Spacecraft Systems Virtual Institute, 2021. *NASA/TP—20210021263 State-of-the-Art of Small Spacecraft Technology*. [Online] Available at: https://www.nasa.gov/sites/default/files/atoms/files/soa_2021_1.pdf [Accessed 30 January 2023].

National Weather Service, 2020. *Hello Solar Cycle 25*. [Online] Available at: <https://www.weather.gov/news/201509-solar-cycle> [Accessed 28 May 2023].

Sivakandan, M., Otsuka, Y., Ghosh, P., Shinagawa, H., Shinbori, A. & Miyoshi, Y., 2021. Comparison of seasonal and longitudinal variation of daytime MSTID activity using GPS observation and GAIA simulations. *Earth, Planets and Space*, 73(35), <https://doi.org/10.1186/s40623-021-01369-5>.

Retterer, J. M., 2010. Forecasting low-latitude radio scintillation with 3-D ionospheric plume models: 1. Plume model. *Journal of Geophysical Research*, Volume 115, A03306, doi:10.1029/2008JA013839.

Smith, J., and Heelis, R. A., 2017. Equatorial plasma bubbles: Variations of occurrence and spatial scale in local time, longitude, season, and solar activity, *Journal of Geophysical Research Space Physics*, 122, 5743– 5755, doi:10.1002/2017JA024128.

Smith, J. M., Rodrigues, F. S., Fejer, B. G. & Milla, M. A., 2016. Coherent and incoherent scatter radar study of the climatology and day-to-day variability of mean F region vertical drifts and equatorial spread F. *Journal of Geophysical Research Space Physics*, Volume 121, pp. 1466 - 1482, <https://doi.org/10.1002/2015JA021934>.

Su, S.-Y., Chao, C. & Liu, C., 2008. On monthly/seasonal/longitudinal variations of equatorial irregularity occurrences and their relationship with the postsunset vertical drift velocities. *Journal of Geophysical Research*, A05307, <https://doi.org/10.1029/2007JA012809>.

Sultan, P. J., 1996. Linear theory and modeling of the Rayleigh-Taylor instability leading to the occurrence of equatorial spread F. *Journal of Geophysical Research*, Volume 101, pp. 26875-26891, <https://doi.org/10.1029/96JA00682>.

Takahashi, H., Wrasse, C.M., Figueiredo, C.A.O.B., Barros, D., Abdu, M.A., Otsuka, Y. & Shiokawa, K., 2018. Equatorial plasma bubble seeding by MSTIDs in the ionosphere. *Progress in Earth and Planetary Science*, 5(32), <https://doi.org/10.1186/s40645-018-0189-2>.

Tsunoda, R. T., 1985. Control of the seasonal and longitudinal occurrence of equatorial scintillations by the longitudinal gradient in integrated E region Pedersen conductivity. *Journal of Geophysical Research*, Volume 90, pp. 447 - 456, doi:10.1029/JA090iA01p00447.

Tsunoda, R. T., Nguyen, T. T. & Le, M. H., 2015. Effects of tidal forcing, conductivity gradient, and active seeding on the climatology of equatorial spread F over Kwajalein. *Journal of Geophysical Research Space Physics*, Volume 120, pp. 632 - 653, doi:10.1002/2014JA020762.

Zou, L., Rishbeth, H., Müller-Wodarg, I.C.F., Aylward, A.D., Millward, G.H., Fuller-Rowell, T.J., Idenden, D.W. & Moffett, R.J., 2000. Annual and semiannual variations in the ionospheric F2-layer. I. Modelling. *Annales Geophysicae*, pp. 927 - 944, <https://doi.org/10.1007/s00585-000-0927-8>.

Declaration of interests

The authors declare that they have no known competing financial interests or personal relationships that could have appeared to influence the work reported in this paper.

The authors declare the following financial interests/personal relationships which may be considered as potential competing interests:

Loren C. Chang reports financial support was provided by National Science and Technology Council, Taiwan. Loren C. Chang reports financial support was provided by Ministry of Education, Taiwan.

Journal Pre-proofs